Upper branch magnetism in quantum magnets: Collapses of excited levels and emergent selection rules

Changle Liu,[1] Fei-Ye Li,[1] and Gang Chen[1,2,*]

[1]*State Key Laboratory of Surface Physics and Department of Physics, Fudan University, Shanghai 200433, China*

[2]*Department of Physics and Center of Theoretical and Computational Physics, The University of Hong Kong, Pokfulam Road, Hong Kong, China*

(Received 14 December 2018; revised manuscript received 9 April 2019; published 5 June 2019)

In many quantum magnets, especially the rare-earth ones, the low-lying crystal-field states are not well separated from the excited ones and thus they are insufficient to describe the low-temperature magnetic properties. Inspired by this simple observation, we develop a microscopic theory to describe the magnetic physics due to the collapses of the weak crystal-field states. We find two cases in which the excited crystal-field states should be seriously included in the theory. One case is when the bandwidth of the excited crystal-field states is comparable to the crystal-field gap. The other case is when the exchange-energy gain between the low-lying and the excited crystal-field states overcomes the crystal-field gap. Both cases could drive a phase transition and result in magnetic orders by involving the excited crystal-field states. We dub the above physics "upper branch magnetism and phase transition." We discuss the multitude of magnetic phases and the emergent selection rules for the detection of the underlying excitations. We expect that our results will help improve the understanding of many rare-earth magnets with weak crystal-field gaps such as $Tb_2Ti_2O_7$ and $Tb_2Sn_2O_7$, and will also provide a complementary perspective to the prevailing local "J" physics in $4d/5d$ magnets.

DOI: 10.1103/PhysRevB.99.224407

I. INTRODUCTION

Frustrated quantum magnetism has been a rather active field of research, both theoretically and experimentally [1,2]. The interest not only lies in the possibility of searching for a novel quantum phase of matter and the related phenomena [1–5], but also arises from the vast families of quantum materials with frustrated magnetic interactions [1,3,6–8]. This prosperous field requires both a microscopic understanding of quantum materials and their quantum chemistry and a theoretical understanding of abstract and fundamental concepts for quantum matter. More importantly, it establishes a bridge between fundamental theories and experimental phenomena. The first step in a theoretical understanding of these complex quantum magnets is to understand the microscopic degrees of freedom. For (magnetic) Mott insulators, the conventional recipe is based on Hund's rules that clarify the microscopic local moment structure [9]. From the interaction of the local moments, one can then establish a microscopic many-body model for the system.

For the rare-earth based quantum magnets that are currently under active study [3,6,7], the crystal-field effect is an important ingredient in the understanding of microscopics. The widely accepted standard approach is to understand the crystal-field level and find the local ground states [9]. The local ground states can be trivial singlets, usual Kramers doublets [10–18], dipole-octupole doublets [19–25], non-Kramers doublets [26–33], triplets, quartets, and so on depending on the symmetry of the crystal-field environment and the nature of magnetic ions, and these local ground states control the low-temperature magnetic properties of many rare-earth magnets. This standard approach has found great success in the study of rare-earth pyrochlore magnets such as $Yb_2Ti_2O_7$ [10,15,34,35] and $Er_2Ti_2O_7$ [35–39], rare-earth triangular magnets such as $YbMgGaO_4$ [13,40–53], and rare-earth-based double perovskites [54]. The local moment structure of the iridate family such as hyper-kagome $Na_4Ir_3O_8$ [55–57], honeycomb Na_2IrO_3 [58–60], hyper-honeycomb β-Li_2IrO_3 [61], and harmonic-honeycomb Li_2IrO_3 [62] may also be interpreted under this scheme. The success of this approach requires that the crystal-field gap between the ground-state doublet and the excited one be sufficiently large. This requirement, however, may not always be satisfied in many systems. In this paper, we provide a nonstandard approach to understand the magnetic physics for systems when the crystal-field gap is not so large. For our purposes, we include the excited crystal-field levels and consider the interactions between these levels from different lattice sites. At the same time, we consider the hybridization between the excited levels and the ground-state level from the neighboring sites. From these ingredients in the microscopic analysis, we illustrate this theoretical framework by applying it to a specific example on a face-centered-cubic (fcc) lattice. Because the magnetic physics emerges from the excited energy levels, we dub this piece of physics "upper branch magnetism."

The remaining part of the paper is organized as follows. In Sec. II, we first introduce our microscopic model for the specific case that we consider. In Sec. III, we use both the Weiss mean-field method and the flavor wave theory to establish the full phase diagram of this model, and we explain the magnetic excitations. In Sec. IV, we explain the emergent selection

*gangchen.physics@gmail.com

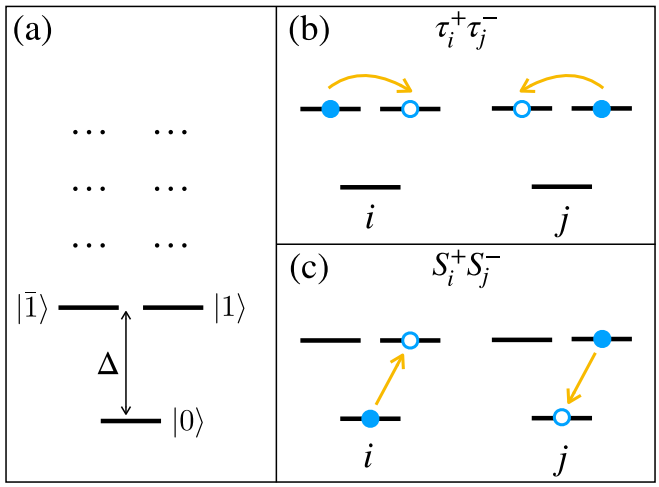

FIG. 1. (a) The crystal-field level scheme for a magnetic ion on a lattice. The lowest three states are viewed as an effective spin-1 local moment. "Δ" is the crystal-field gap. "$\cdots$" refers to the excited doublets that are neglected in our theoretical analysis. (b) The $\tau_i^+\tau_j^-$ process. (c) One of the possible $S_i^+S_j^-$ processes, i.e., $S_i^+S_j^-|0\rangle_i|1\rangle_j = |1\rangle_i|0\rangle_j$.

rules for the detection of magnetic excitations. This is associated with certain symmetry properties of the ground-state wave functions of the relevant magnetic phases. In Sec. V, we conclude with a discussion about the general applicability of our understanding to weak crystal-field quantum magnets, and we present a list of systems and materials that share some similarities in terms of local energy level schemes, phase transitions, and universality.

II. MICROSCOPIC MODEL

The magnetic physics from the weak crystal-field levels is quite general and applies to many different systems with different lattice geometries. To illustrate the essential physics, we focus on only one lattice. We study the interacting local moments with weak crystal fields on the fcc lattice. To further simplify the model and maintain the essential physics, we consider the local crystal-field level scheme in Fig. 1. The local ground state here is a singlet, and the first excited state is a doublet. This crystal-field scheme could occur for the rare-earth ion with an even number of electrons [63,64]. For the rare-earth ion with an odd number of electrons, the ground state must at least be a doublet (although the possibility of being a quartet may still remain), and one then needs to consider the interaction between these doublets. This would complicate the problem and cover the essential physics that is uncovered in this work.

If the crystal-field gap, Δ, is much larger than other energy scales that are specified below, the ground state of the system would be a trivial product state of the local singlets. There are other microscopic processes that compete with the crystal-field gap. As we show in Fig. 1, one process is the superexchange interaction between the upper doublets. The other process is the hybridization between the ground state and the excited doublet. Fundamentally, both processes arise from the superexchange interactions. To distinguish them, however, we quote them differently.

To model the minimal microscopic physics, we neglect any additional excited states beyond the three states in Fig. 1. The three states, one ground-state singlet and one excited doublet, can be thought of as an effective spin-1 local moment. We identify the ground-state singlet as the $S^z = 0$ state, and the excited doublet as $S^z = \pm 1$ states. From this mapping, the crystal-field splitting can be regarded as a single-ion anisotropy, i.e.,

$$H_{\mathrm{CEF}} = \Delta \sum_i \left(S_i^z\right)^2. \tag{1}$$

The superexchange interaction between the upper doublet is given as

$$H_{\mathrm{ex}} = \sum_{\langle ij\rangle} J_{zz}\tau_i^z\tau_j^z - J_\perp(\tau_i^+\tau_j^- + \mathrm{H.c.}) + \cdots, \tag{2}$$

where the pseudospin-1/2 operator $\boldsymbol{\tau}_i$ operates on the upper doublet. For strong spin-orbit coupled systems, there are also other types of doublet interactions (denotes as "$\cdots$") such as $\tau_i^+\tau_j^+$ and $\tau_i^-\tau_j^-$ that are allowed by symmetry and should be presented in the Hamiltonian. However, here we only consider XXZ-type interactions and omit these terms for simplicity.

It is straightforward to establish the following relation between the pseudospins and the spin-1 operators:

$$\tau_i^z \equiv \tfrac{1}{2}P_iS_i^zP_i, \tag{3}$$

$$\tau_i^\pm \equiv \tfrac{1}{2}P_i(S_i^\pm)^2P_i, \tag{4}$$

where P_i is a projection operator onto the upper doublet.

We introduce the hybridization as a conventional superexchange, i.e.,

$$H_{\mathrm{hybrid}} = -\sum_{\langle ij\rangle} J_h(S_i^+S_j^- + S_i^-S_j^+). \tag{5}$$

Summarizing the above results, we have our full minimal model as $H = H_{\mathrm{CEF}} + H_{\mathrm{ex}} + H_{\mathrm{hybrid}}$. This model hosts a $U(1)$ symmetry generated by spin rotation of an arbitrary angle about the z axis. This continuous symmetry is due to an oversimplification of our model, and it is expected to vanish for realistic materials with strong spin-orbit coupling.

Here our model has effective spin-1 degrees of freedom, which potentially support more kinds of orders than usual spin-1/2 systems. It is well known that for spin-1 systems, there are altogether eight nontrivial linearly independent operators that act on the local Hilbert space, namely S^μ and $Q^{\mu\nu} \equiv \frac{1}{2}(S^\mu S^\nu + S^\nu S^\mu) - \frac{2}{3}\delta_{\mu\nu}$ $(\mu, \nu = x, y, z)$. The expectation values of these operators can be used to characterize the orders in different phases. Here, we mention that while $\boldsymbol{S}$ and $\tau^\pm = \frac{1}{2}(Q^{xx} - Q^{yy}) \pm 2iQ^{xy}$ can be served as symmetry-breaking order parameters, the operator $Q^{zz} = (S^z)^2 - \frac{2}{3}$ cannot be served as an order parameter as the crystal-field splitting term $(S^z)^2$ explicitly enters the Hamiltonian.

The further question is how to detect these orders experimentally. To answer this question, we have to look into the physical nature of these orders. Generally, the answer depends on the symmetry of the crystal field and the details of crystal-field wave functions. Here we consider the situation in

TABLE I. Physical properties of different magnetic phases. Both the FM_{xy} state and the FQ_{xy} state have a $U(1)$ degeneracy characterized by the angular variable θ. For the FM_{xy} state, $c^2 \equiv (48J_h - \Delta)/(192J_h)$. Note that when $J_h/\Delta = 1/48$, we have $c = 0$, $|\Psi\rangle_i = |0\rangle$, and when $J_h \to \infty$ we have $c = 1/2$; $|\Psi\rangle_i$ becomes fully polarized in the xy plane.

Magnetic phases	Dipoles	Quadrupoles	Local variational wave function	Variational energy per site
Quantum paramagnet	$\langle \boldsymbol{S}\rangle = \boldsymbol{0}$	$\langle \tau^{\pm}\rangle = 0$	$\|0\rangle$	0
FM_{xy}	$\langle S^{\pm}\rangle \neq 0$	$\langle \tau^{\pm}\rangle = 0$	$c\,e^{i\theta}\|1\rangle + \sqrt{1-2c^2}\,\|0\rangle + c\,e^{-i\theta}\|\bar{1}\rangle$	$-192c^4J_h$
FM_z	$\langle S^z\rangle \neq 0$	$\langle \tau^{\pm}\rangle = 0$	$\|1\rangle$ or $\|\bar{1}\rangle$	$\frac{3J_{zz}}{2} + \Delta$
AFM_z	$\langle S^z\rangle \neq 0$	$\langle \tau^{\pm}\rangle = 0$	$\|e^{i\boldsymbol{Q}\cdot\boldsymbol{r}_i}\rangle$ with $\boldsymbol{Q} = (0, 0, 2\pi)$	$-\frac{J_{zz}}{2} + \Delta$
FQ_{xy}	$\langle \boldsymbol{S}\rangle = \boldsymbol{0}$	$\langle \tau^{\pm}\rangle \neq 0$	$\frac{1}{\sqrt{2}}(e^{i\theta/2}\|1\rangle + e^{-i\theta/2}\|\bar{1}\rangle)$	$-3J_{\perp} + \Delta$

which the crystal field has a D_{3d} or O_h point group symmetry, as both cases are consistent with fcc structure and support the singlet-doublet crystal-field scenario that we proposed here. In both cases, the doublet crystal-field levels carry an E_g irreducible representation, while the singlet level carries either an A_{1g} or A_{2g} representation. For both cases, all effective spin components S^{μ} are time-reversal odd and behave as dipole moments, similar to usual spins. The dipolar order directly couples to neutrons, thus it can be visible in elastic neutron-scattering experiments. Meanwhile, the spin-bilinear components $Q^{\mu\nu}$ behave as quadrupoles that are even under time reversal, therefore they are often not quite visible in such conventional experimental probes. We will discuss the experimental relevance further in Sec. IV.

III. PHASE DIAGRAM

A. Weiss mean-field theory

To establish the ground-state phase diagram of the full model, we adopt the Weiss mean-field method to decouple interactions between different sites. The Weiss mean-field approach is essentially a variational approach with simple product states as the variational wave function. We express here the trial ground-state wave function as a product state,

$$|\Psi_{GS}\rangle = \prod_i |\Psi\rangle_i. \tag{6}$$

To take the antiferromagnetic (AFM) ordering into account, here we set up a two-sublattice ansatz, i.e., $|\Psi\rangle_i = |\Psi\rangle_A(|\Psi\rangle_B)$, when site i belongs to the sublattice A (B). Here $|\Psi\rangle_A$ and $|\Psi\rangle_B$ are independent single-site wave functions. The A (B) sublattice is chosen exactly as the up (down) spin sites in an AFM spin configuration on the fcc lattice with wave vector $\boldsymbol{Q} = (0, 0, 2\pi)$. This type of AFM ordering is a common order pattern on an antiferromagnetically interacting fcc magnet. The single-site state $|\Psi\rangle_i$ is then determined by minimizing the energy per site $E = \langle\Psi_{GS}|H|\Psi_{GS}\rangle/N_{site}$. The results are listed in Table I using the S^z diagonal basis $|S^z = 1, 0, \bar{1}\rangle$. Our mean-field phase diagram is shown in Fig. 2. We can understand the magnetic phases with interactions involving upper branch (excited) states. The corresponding order parameters for different phases are listed in Table I.

In the large Δ limit where the crystal-field gap is dominant, the ground state is a trivial product state of a nonmagnetic singlet on each lattice site, which we dub the "quantum paramagnetic state." Such a state is protected by the energy gap Δ and hence is stable against small perturbations. When the interactions in H_{ex} and H_{hybrid} become large enough such that the energy gain from the exchange or hybridization overcomes the crystal-field gap, various magnetic orders can be realized. The J_z term favors spins to form a dipolar order along the z axis, leading to the FM_z (AFM_z) state in the left (right) side of the quantum paramagnetic state [see Figs. 2(a) and 2(b)]. Similarly, the $J_{\perp}$ term favors the dipolar order with spins on the xy plane. This gives the FM_{xy} state in the upper side of Fig. 2(a). Finally, the hybridization term J_h favors spins to form quadrupolar order with the director of the quadrupolar order on the xy plane, giving the FQ_{xy} state in the upper part of Fig. 2(b). Both the FM_{xy} and FQ_{xy} states spontaneously

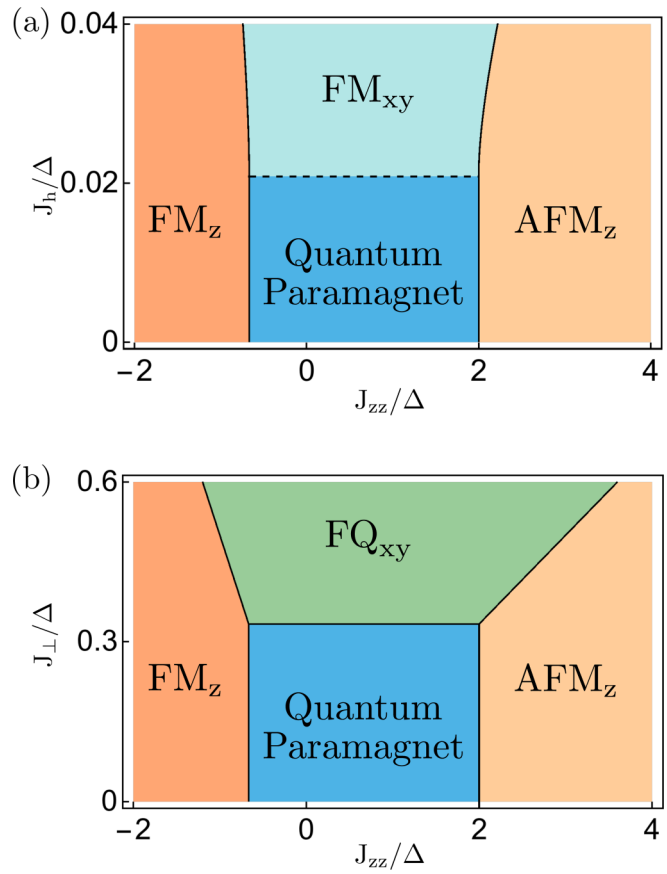

FIG. 2. Phase diagram for (a) $J_{\perp} = 0$ and (b) $J_h = 0$. The details of the ordered phases are explained in the main text. The dashed line in (a) refers to a continuous phase transition and the remaining transitions are first-order.

break the global $U(1)$ symmetry. The details of these states can be found in Table I.

Although both $H_{\rm ex}$ and $H_{\rm hybrid}$ could drive the system out of the quantum paramagnetic state, the mechanisms in which the excited levels are involved are quite different. For the former case, the neighboring magnetic states are driven by exchange terms through first-order transitions, reflecting the competition between the crystal-field splitting and the exchange energy gain purely within the excited levels through, for example, the $\tau_i^+\tau_j^-$ process shown in Fig. 1(b). For the latter case, however, the hybridization term drives the system into the $\mathrm{FQ_{xy}}$ state through a continuous transition. The excited states can hop between different sites via the hybridization processes, and one such process is shown in Fig. 1(c). $H_{\rm hybrid}$ hence introduces the bandwidth to the excited states, and the criticality is obtained when the bandwidth is comparable with the crystal-field gap. To further clarify this point, we study the instability of the quantum paramagnetic state from the flavor wave theory below.

B. Flavor wave theory and magnetic excitations

We adopt the flavor wave theory to investigate the spin excitations and reveal the magnetic instability of the quantum paramagnetic state [65]. Within this framework, different roles that are played by $H_{\rm ex}$ and $H_{\rm hybrid}$ will be clear.

Under the flavor wave representation, the internal states of a spin at site i are represented by three flavors of bosons,

$$b_{im}^\dagger|\Omega\rangle \equiv \left|S_i^z = m\right\rangle, \tag{7}$$

where $|\Omega\rangle$ represents the vacuum state. An arbitrary on-site spin operator O_i can be written as $\sum_{m,n}\langle m|O|n\rangle b_{im}^\dagger b_{in}$ with $m, n = 1, 0, \bar{1}$. The physical Hilbert space is recovered under the local Hilbert space constraint $\sum_m b_{im}^\dagger b_{im} = 1$.

In the following, we will omit the site index i for simplicity. The relevant on-site spin operators can be written as

$$\tau^z = \tfrac{1}{2}(b_1^\dagger b_1 - b_{\bar{1}}^\dagger b_{\bar{1}}), \tag{8}$$

$$\tau^+ = b_1^\dagger b_{\bar{1}}, \quad \tau^- = b_{\bar{1}}^\dagger b_1, \tag{9}$$

$$(S^z)^2 = b_1^\dagger b_1 + b_{\bar{1}}^\dagger b_{\bar{1}}, \tag{10}$$

$$S^+ = \sqrt{2}(b_1^\dagger b_0 + b_0^\dagger b_{\bar{1}}), \tag{11}$$

$$S^- = \sqrt{2}(b_{\bar{1}}^\dagger b_0 + b_0^\dagger b_1). \tag{12}$$

In the language of the flavor wave theory, different magnetic phases can be obtained by condensing corresponding flavors of the bosons. For the quantum paramagnet of this subsection, the b_0 flavor is condensed and

$$b_{i0}^\dagger = b_{i0} \simeq [1 - b_{i1}^\dagger b_{i1} - b_{i\bar{1}}^\dagger b_{i\bar{1}}]^{1/2}, \tag{13}$$

while the other two flavors of bosons represent the excited states above the quantum paramagnetic state. The (quadratic) flavor wave Hamiltonian is then obtained as

$$H = \sum_{\boldsymbol{k}} \Psi_{\boldsymbol{k}}^\dagger \begin{pmatrix} B_{\boldsymbol{k}} + \Delta & B_{\boldsymbol{k}} \\ B_{\boldsymbol{k}} & B_{\boldsymbol{k}} + \Delta \end{pmatrix} \Psi_{\boldsymbol{k}}, \tag{14}$$

where $\Psi_{\boldsymbol{k}} = (b_{\boldsymbol{k}1}, b_{-\boldsymbol{k}\bar{1}}^\dagger)^T$ and $B_{\boldsymbol{k}} = -2J_h\gamma_{\boldsymbol{k}}$, with $\gamma_{\boldsymbol{k}} = \sum_{\boldsymbol{\delta}} \cos(\boldsymbol{k}\cdot\boldsymbol{\delta})$, and $\boldsymbol{\delta}$ is summed over the 12 nearest-neighbor vectors of the fcc lattice. The magnetic excitation with respect to the quantum paramagnetic state has a twofold degeneracy that is protected by the time-reversal symmetry of the quantum paramagnet. The dispersion of the magnetic excitations is

$$\omega_{\boldsymbol{k}} = [\Delta(2B_{\boldsymbol{k}} + \Delta)]^{1/2}. \tag{15}$$

The magnetic excitations are fully gapped inside the quantum paramagnetic state. As the system approaches the transition to a proximate ordered phase, the gap of the excitation is closed. The closing point is at the Γ point and $J_h = \Delta/48$. At this critical point, the excitation spectrum disperses linearly near the Γ point, contributing to a $C_v \sim T^3$ heat capacity behavior at low temperatures.

It is apparent that the (quadratic) flavor wave Hamiltonian depends on J_h while it does not depend on J_z or $J_\perp$. As we have previously discussed, the hybridization term J_h would create quantum fluctuations above the quantum paramagnetic state and bring the dispersion to the excitation crystal-field state. However, the exchange part $H_{\rm ex}$ only acts within the upper branch excited states and does not mix the upper branches with the local crystal-field ground state. Therefore, the induced transitions from the quantum paramagnet to ordered states through $H_{\rm ex}$ must be strongly first-order.

C. Flavor wave theory for the $\mathrm{FM_{xy}}$ state

For the $\mathrm{FM_{xy}}$ state, we choose the magnetization along the $\hat{x}$ direction to break the continuous $U(1)$ symmetry such that the variational wave function has the form

$$|\Psi\rangle_i = c\,|1\rangle + \sqrt{1-2c^2}\,|0\rangle + c\,|\bar{1}\rangle. \tag{16}$$

We introduce a new basis for the three flavors of bosons via a unitary transformation,

$$\begin{pmatrix} a_0 \\ a_1 \\ a_2 \end{pmatrix} = \begin{pmatrix} c & \sqrt{1-2c^2} & c \\ \frac{i}{\sqrt{2}} & 0 & -\frac{i}{\sqrt{2}} \\ i\sqrt{\frac{1-2c^2}{2}} & -i\sqrt{2}c & i\sqrt{\frac{1-2c^2}{2}} \end{pmatrix} \begin{pmatrix} b_1 \\ b_0 \\ b_{\bar{1}} \end{pmatrix}, \tag{17}$$

and we condense the a_0 flavor. The quadratic flavor wave Hamiltonian reads

$$H = \frac{1}{2}\sum_{\boldsymbol{k}} \Phi_{\boldsymbol{k}}^\dagger \begin{pmatrix} m_{11} & 0 & m_{13} & 0 \\ 0 & m_{22} & 0 & m_{24} \\ m_{13} & 0 & m_{11} & 0 \\ 0 & m_{24} & 0 & m_{22} \end{pmatrix} \Phi_{\boldsymbol{k}}, \tag{18}$$

where the entries in the matrix are given by

$$m_{11} = (1-2c^2)(192c^2J_h + \Delta) - [4(1-2c^2)J_h - c^2J_{zz}]\gamma_{\boldsymbol{k}}/2, \tag{19}$$

$$m_{13} = -[4(1-2c^2)J_h + c^2J_{zz}]\gamma_{\boldsymbol{k}}/2, \tag{20}$$

$$m_{22} = (1-2c^2)(192c^2J_h + \Delta) - \Delta - 2(1-4c^2)^2J_h\gamma_{\boldsymbol{k}}, \tag{21}$$

$$m_{24} = 2(1-4c^2)^2J_h\gamma_{\boldsymbol{k}}, \tag{22}$$

and $\Phi_{\boldsymbol{k}} \equiv (a_{\boldsymbol{k}1}, a_{\boldsymbol{k}2}, a_{-\boldsymbol{k}\bar{1}}^\dagger, a_{-\boldsymbol{k}\bar{2}}^\dagger)$.

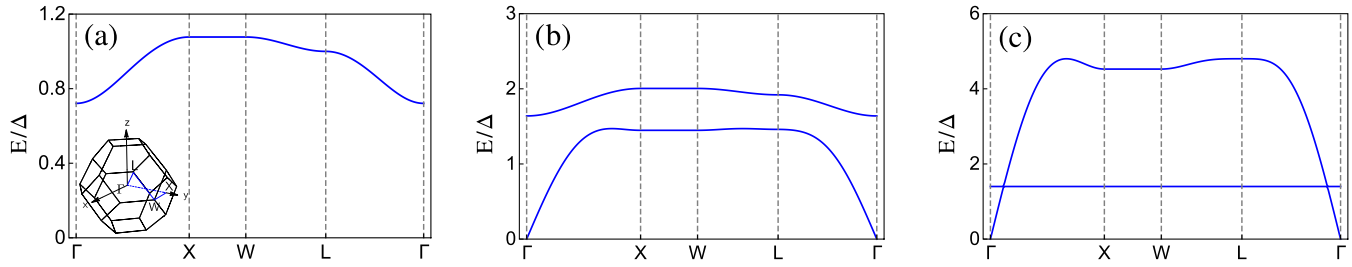

FIG. 3. Flavor wave excitations for (a) the quantum paramagnet, (b) the FM_{xy} state, and (c) the FQ_{xy} state. We set the magnetization of the FM_{xy} state along the $\hat{x}$ direction, and the director of the quadrupolar order in the FQ_{xy} state parallel to the x axis. The parameters are shown in Fig. 4. The inset in (a) indicates the high-symmetry points in the Brillouin zone of the fcc lattice.

D. Flavor wave theory for the FQ_{xy} state

For the FQ_{xy} state, we choose the director of this quadrupolar state along the x axis to break the $U(1)$ rotational symmetry. The single-site variational wave function is given as

$$|\Psi\rangle_i = \frac{i}{\sqrt{2}}(|1\rangle - |\bar{1}\rangle). \tag{23}$$

To describe the elementary excitations with respect to this ground state, we introduce a new basis for the flavors of bosons by the following transformation:

$$\begin{pmatrix} a_0 \\ a_1 \\ a_2 \end{pmatrix} = \begin{pmatrix} \frac{-i}{\sqrt{2}} & 0 & \frac{i}{\sqrt{2}} \\ \frac{1}{\sqrt{2}} & 0 & \frac{1}{\sqrt{2}} \\ 0 & i & 0 \end{pmatrix} \begin{pmatrix} b_1 \\ b_0 \\ b_{\bar{1}} \end{pmatrix}, \tag{24}$$

and we condense the a_0 flavor. The quadratic flavor wave Hamiltonian reads

$$H = \frac{1}{2}\sum_{\boldsymbol{k}} \Phi_{\boldsymbol{k}}^{\dagger} \begin{pmatrix} m_{11} & 0 & m_{13} & 0 \\ 0 & m_{22} & 0 & m_{24} \\ m_{13} & 0 & m_{11} & 0 \\ 0 & m_{24} & 0 & m_{22} \end{pmatrix} \Phi_{\boldsymbol{k}}, \tag{25}$$

where the matrix entries are given as

$$m_{11} = 12J_{\perp} - \gamma_{\boldsymbol{k}}(2J_{\perp} - J_{zz})/4, \tag{26}$$

$$m_{13} = -\gamma_{\boldsymbol{k}}(2J_{\perp} + J_{zz})/4, \tag{27}$$

$$m_{22} = 6J_{\perp} - \Delta, \tag{28}$$

$$m_{24} = 0, \tag{29}$$

and $\Phi_{\boldsymbol{k}} \equiv (a_{\boldsymbol{k}1}, a_{\boldsymbol{k}2}, a^{\dagger}_{-\boldsymbol{k}\bar{1}}, a^{\dagger}_{-\boldsymbol{k}\bar{2}})$.

IV. EMERGENT SELECTION RULES

A. Selective measurements of dipole and quadrupole moments

In conventional experimental measurements such as neutron and μSR, one can only probe the dipolar orders while the quadrupolar orders are not directly visible in conventional magnetic measurements. The question thus arises of how to experimentally detect the phases accompanied by quadrupole components in our phase diagram. In previous works, some of the authors have proposed the scheme of selective measurements of dipole and quadrupole components using elastic and inelastic probes [21,33,66], and a similar approach can be used here. The dipole moment, $\boldsymbol{S}$, is directly visible through conventional magnetic measurements such as NMR and elastic neutron experiment. Since the quadrupole moments do not commute with dipolar ones along orthogonal directions, when the neutron scattering measures the dipole components, it creates quantum fluctuations to the orthogonal quadrupoles, leading to coherent spin-wave-like excitations. This means that although the quadrupole itself is invisible in a usual neutron-scattering measurement, the dynamic excitations of quadrupolar orders can be visible in experiments, and these excitations carry information of the underlying quadrupole structure.

To demonstrate the above discussion, we calculate the magnetic excitations and the dynamic spin structure factors for three representative states in Fig. 2 using the flavor wave theory. The results are shown in Figs. 3 and 4. In the polarized inelastic neutron-scattering experiment, one measures the dynamic spin structure factors

$$\mathcal{S}^{\mu\nu}(\boldsymbol{k},\omega) = \frac{1}{2\pi N}\sum_{ij}\int_{-\infty}^{+\infty} dt\, e^{i\boldsymbol{k}\cdot(\mathbf{r}_i-\mathbf{r}_j)-i\omega t}\left\langle S_i^{\mu}(0)S_j^{\nu}(t)\right\rangle, \tag{30}$$

where $\mu, \nu = x, y, z$ represent the polarizations of incoming and scattered neutrons. Thus one can read off signatures of the dipole and quadrupole components separately from the elastic and inelastic probes.

B. Emergent selection rules

In the plot of relevant dynamic spin structure factors in Fig. 4, the two branches of magnetic excitations in the quantum paramagnet are degenerate due to the time-reversal symmetry, while only one branch of magnetic excitations in the FM_{xy} and FQ_{xy} states is visible. As we show below, the latter arises from the emergent selection rules.

We start with the FM_{xy} state. For this state, the elastic neutron scattering is able to reveal an in-plane ferromagnetic dipolar order (e.g., along the $\hat{x}$ direction for the choice in the previous section). For the usual ferromagnet for spin-1/2 degrees of freedom, the dynamic spin structure factor for spin components along the ferromagnetic ordering direction measures the two-magnon continuum. For our effective spin-1 local moments that have a larger physical Hilbert space, the microscopic interaction in the Hamiltonian could access the large Hilbert space at the linear order. This qualitatively

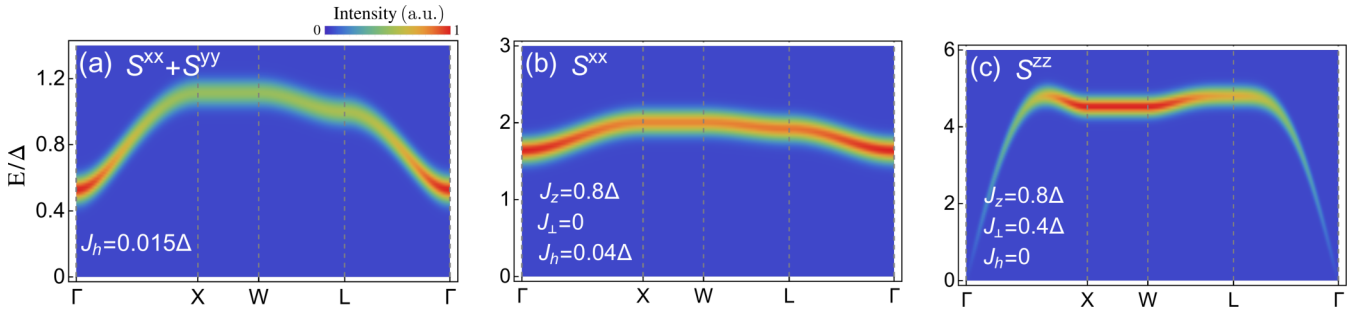

FIG. 4. Dynamic spin structure factors of (a) the quantum paramagnet, (b) the FM_{xy} state, and (c) the FQ_{xy} state. All three states have nonvanishing quadrupole components that can be detected via inelastic neutron-scattering measurements with corresponding polarization channels. Only coherent excitations are considered here. Please see the full spectra of the flavor wave excitations in Fig. 3 as a comparison.

explains the presence of coherent magnetic excitation in Fig. 4(b). More specifically, within the flavor wave theory, the S^x operator in the reciprocal space is written as

$$S^x_{\boldsymbol{k}} = i(1-4c^2)(a_{k2} - a^\dagger_{-k2}), \tag{31}$$

where the static piece for the ferromagnetic order has been ignored.

The absence of one branch of magnetic excitation in Fig. 4(b) is a consequence of the emergent selection rule. Our Hamiltonian is invariant under the following $\mathbb{Z}_2$ symmetry operations generated by

$$\hat{G}_x = e^{-i\pi \sum_j (S^x_j + 1)}, \tag{32}$$

$$\hat{G}_y = e^{-i\pi \sum_j (S^y_j + 1)}. \tag{33}$$

For the FM_{xy} state, we have chosen the dipolar magnetization along the $\hat{x}$ direction such that the $\hat{G}_x$ symmetry is preserved. The flavor wave operators a_1 and a_2 (in Sec. III C) are odd and even under $\hat{G}_x$, respectively. Therefore, the S^x operation only excites the a_2 flavor with even parity while the a_1 band that has odd parity is hidden in this measurement.

The same strategy can be applied to the FQ_{xy} state (we have chosen the quadrupolar director along the x axis), but we need to consider the $\hat{G}_y$ symmetry. Following the same argument, one can see that in the S^{zz} channel only odd-parity a_1 excitation can be measured in the spectrum. More explicitly, the S^z operator is written as

$$S^z_{\boldsymbol{k}} = -i(a_{k1} - a^\dagger_{-k1}) \tag{34}$$

in the flavor wave formulation of Sec. III D.

V. DISCUSSION

In summary, we have explored the physical consequences of weak crystal-field splitting for which the standard approach is insufficient to capture the low-energy magnetic physics. For concreteness, we study a model system with the weak crystal-field level scheme on the fcc lattice. Using the Weiss mean-field method, we obtain the phase diagram of this model. We also adopt the flavor wave theory to obtain the magnetic excitations and reveal the effects of the excited crystal-field states. There are two different mechanisms from which various magnetic ordering happens. One is related to the exchange within the excited levels and the other is related to the hybridization between the ground-state level and the excited levels. The fcc lattice may not be highly frustrated, and the states are mostly ordered in our study. On more frustrated lattices, the collapses of the excited crystal-field states may lead to more possibilities such as a quantum spin liquid.

As for the physical relevance, we are currently not aware of many relevant physical systems that explicitly show the upper branch magnetism. The pyrochlore material $Tb_2Ti_2O_7$ (and maybe other Tb-based pyrochlore magnets, e.g., $Tb_2Sn_2O_7$) [63,75–82] can be thought of as a potential relevance, except that the local ground state for the Tb^{3+} ion is a doublet. The crystal-field gap is not as large as other well-known pyrochlore magnets such as $Yb_2Ti_2O_7$ or $Er_2Ti_2O_7$. For example, Ref. [80] actually measured a 4 gap of 1.5 meV between the ground-state doublet and the excited-state doublet in $Tb_2Ti_2O_7$. This gap is comparable to the Curie-Weiss temperature and the bandwidth of the magnetic excitations [80]. Thus, the usage of the effective spin-1/2 local moment for the ground-state doublet of the Tb^{3+} ion may not apply very well in certain cases. The magnetic entropy of $Tb_2Sn_2O_7$ does increase beyond $R\ln 2$ as the temperature is increased beyond 4 K [81]. The inelastic neutron scattering measurement in $Tb_2Ti_2O_7$ shows a clear dispersion for the excited doublets with a renormalized gap [83]. All these phenomena suggest the importance of the upper branch physics. It would be interesting in the future to actually suppress the weak crystal-field gap and drive the system to magnetic orders by collapsing the excited levels. In fact, $Tb_2Sn_2O_7$ experiences a magnetic ordering transition around 1 K [81]. The actual modeling of the magnetic physics should be in terms of an effective $J = 3/2$ local moment that takes care of both the ground-state doublet and the first excited-state doublet, and the interaction would naturally be a Γ-matrix model.

For the $4d/5d$ magnets such as iridates and others, the often used description is in terms of the spin-orbit-entangled local moment J [84]. This should certainly be the case if the local ground state J is well separated from the excited J states. The $4d/5d$ orbitals, however, are very extended. Very often, the hybridization of the superexchange involving the upper excited J states may not be that small compared to the local energy gap due to the spin-orbit coupling. This piece of physics has been nicely invoked by Khaliullin in Ref. [70] for the $4d^4/5d^4$ magnets, where he described the physics as the singlet-triplet condensation to make the analogy with the triplon condensation in the dimerized magnets. Here we

TABLE II. List of physical contexts that support similar upper branch physics. "Relevant condensation" in the table refers to either a field driven or an exchange interaction driven transition.

Systems and Materials	Local Low-lying States	Relevant Condensation	Refs
Dimerized magnets	Singlet of two neighboring spins	Triplon from the triplets	Ref. [67]
A-site spinel $FeSc_2S_4$	Spin-orbital singlet with e_g orbitals	Spin-orbital excited states	Refs. [68,69]
$4d^4/5d^4$ Mott insulators (Ca_2RuO_4)	Spin-orbital singlet with t_{2g} orbitals	Spin-orbital excitons	Refs. [70–73]
$3d^8/4d^8$ Mott insulators	Spin-orbital singlet with t_{2g} orbitals	Spin-orbital excitons	Ref. [74]
Magnets with weak crystal-field gaps	Local low-lying crystal-field state	Excited crystal-field states	This work

think this physics is not restricted to the $4d^4/5d^4$ magnets whose local ground state would be a trivial spin-orbit singlet with $J = 0$, but extends broadly to many other nonsinglet spin-orbit-coupled magnets (as long as the spin-orbit-coupling induced local gap is not large).

In Table II, we list the relevant systems/materials that could share a similar physics to the upper branch physics in this work. Our result simply provides an additional member to this list of "triplon"-like physics. We expect that the universal physics like the Higgs mode (or the amplitude mode) could also emerge in the relevant materials of our work where the condensation or criticality is from the collapse of the excited crystal-field states.

ACKNOWLEDGMENTS

This work was supported by the Ministry of Science and Technology of China under Grants No. 2016YFA0301001, No. 2016YFA0300500, and No. 2018YFGH000095.

C.L. and F.-Y.L. contributed equally to this work.

[1] L. Balents, Spin liquids in frustrated magnets, Nature (London) **464**, 199 (2010).

[2] R. Moessner, Magnets with strong geometric frustration, Can. J. Phys. **79**, 1283 (2001).

[3] L. Savary and L. Balents, Quantum spin liquids: A review, Rep. Prog. Phys. **80**, 016502 (2017).

[4] P. A. Lee, An end to the drought of quantum spin liquids, Science **321**, 1306 (2008).

[5] M. R. Norman, Colloquium: Herbertsmithite and the search for the quantum spin liquid, Rev. Mod. Phys. **88**, 041002 (2016).

[6] M. J. P. Gingras and P. A. McClarty, Quantum spin ice: A search for gapless quantum spin liquids in pyrochlore magnets, Rep. Prog. Phys. **77**, 056501 (2014).

[7] J. S. Gardner, M. J. P. Gingras, and J. E. Greedan, Magnetic pyrochlore oxides, Rev. Mod. Phys. **82**, 53 (2010).

[8] J. G. Rau and M. J. P. Gingras, Frustrated quantum rare-earth pyrochlores, Annu. Rev. Condens. Matter Phys. **10**, 357 (2019).

[9] P. Fazekas, *Lecture Notes on Electron Correlation and Magnetism*, Series in Modern Condensed Matter Physics: Vol. 5 (World Scientific, Singapore, 1999).

[10] K. A. Ross, L. Savary, B. D. Gaulin, and L. Balents, Quantum Excitations in Quantum Spin Ice, Phys. Rev. X **1**, 021002 (2011).

[11] J. D. Thompson, P. A. McClarty, H. M. Rønnow, L. P. Regnault, A. Sorge, and M. J. P. Gingras, Rods of Neutron Scattering Intensity in $Yb_2Ti_2O_7$: Compelling Evidence for Significant Anisotropic Exchange in a Magnetic Pyrochlore Oxide, Phys. Rev. Lett. **106**, 187202 (2011).

[12] R. M. D'Ortenzio, H. A. Dabkowska, S. R. Dunsiger, B. D. Gaulin, M. J. P. Gingras, T. Goko, J. B. Kycia, L. Liu, T. Medina, T. J. Munsie, D. Pomaranski, K. A. Ross, Y. J. Uemura, T. J. Williams, and G. M. Luke, Unconventional magnetic ground state in $Yb_2Ti_2O_7$, Phys. Rev. B **88**, 134428 (2013).

[13] Y. Li, G. Chen, W. Tong, L. Pi, J. Liu, Z. Yang, X. Wang, and Q. Zhang, Rare-Earth Triangular Lattice Spin Liquid: A Single-Crystal Study of $YbMgGaO_4$, Phys. Rev. Lett. **115**, 167203 (2015).

[14] Y.-D. Li, X. Wang, and G. Chen, Anisotropic spin model of strong spin-orbit-coupled triangular antiferromagnets, Phys. Rev. B **94**, 035107 (2016).

[15] J. G. Rau and M. J. P. Gingras, Frustration and anisotropic exchange in ytterbium magnets with edge-shared octahedra, Phys. Rev. B **98**, 054408 (2018).

[16] A. Scheie, J. Kindervater, S. Säubert, C. Duvinage, C. Pfleiderer, H. J. Changlani, S. Zhang, L. Harriger, K. Arpino, S. M. Koohpayeh, O. Tchernyshyov, and C. Broholm, Reentrant Phase Diagram of $Yb_2Ti_2O_7$ in a 111 Magnetic Field, Phys. Rev. Lett. **119**, 127201 (2017).

[17] A. M. Hallas, J. Gaudet, M. N. Wilson, T. J. Munsie, A. A. Aczel, M. B. Stone, R. S. Freitas, A. M. Arevalo-Lopez, J. P. Attfield, M. Tachibana, C. R. Wiebe, G. M. Luke, and B. D. Gaulin, XY antiferromagnetic ground state in the effective $S = \frac{1}{2}$ pyrochlore $Yb_2Ge_2O_7$, Phys. Rev. B **93**, 104405 (2016).

[18] S. Onoda, Effective quantum pseudospin-1/2 model for Yb pyrochlore oxides, J. Phys.: Conf. Ser. **320**, 012065 (2011).

[19] Y.-P. Huang, G. Chen, and M. Hermele, Quantum Spin Ices and Topological Phases from Dipolar-Octupolar Doublets on the Pyrochlore Lattice, Phys. Rev. Lett. **112**, 167203 (2014).

[20] Y.-D. Li and G. Chen, Symmetry enriched U(1) topological orders for dipole-octupole doublets on a pyrochlore lattice, Phys. Rev. B **95**, 041106(R) (2017).

[21] Y.-D. Li, X. Wang, and G. Chen, Hidden multipolar orders of dipole-octupole doublets on a triangular lattice, Phys. Rev. B **94**, 201114(R) (2016).

[22] E. Lhotel, S. Petit, S. Guitteny, O. Florea, M. Ciomaga Hatnean, C. Colin, E. Ressouche, M. R. Lees, and G. Balakrishnan, Fluctuations and All-In–All-Out Ordering in Dipole-Octupole $Nd_2Zr_2O_7$, Phys. Rev. Lett. **115**, 197202 (2015).

[23] O. Benton, Quantum origins of moment fragmentation in $Nd_2Zr_2O_7$, Phys. Rev. B **94**, 104430 (2016).

[24] J. Xu, V. K. Anand, A. K. Bera, M. Frontzek, D. L. Abernathy, N. Casati, K. Siemensmeyer, and B. Lake, Magnetic structure and crystal-field states of the pyrochlore antiferromagnet $Nd_2Zr_2O_7$, Phys. Rev. B **92**, 224430 (2015).

[25] S. Petit, E. Lhotel, B. Canals, M. Ciomaga Hatnean, J. Ollivier, H. Mutka, E. Ressouche, A. R. Wildes, M. R. Lees, and G. Balakrishnan, Observation of magnetic fragmentation in spin ice, Nat. Phys. **12**, 746 (2016).

[26] S. Onoda and Y. Tanaka, Quantum Melting of Spin Ice: Emergent Cooperative Quadrupole and Chirality, Phys. Rev. Lett. **105**, 047201 (2010).

[27] S. Onoda and Y. Tanaka, Quantum fluctuations in the effective pseudospin-$\frac{1}{2}$ model for magnetic pyrochlore oxides, Phys. Rev. B **83**, 094411 (2011).

[28] S. B. Lee, S. Onoda, and L. Balents, Generic quantum spin ice, Phys. Rev. B **86**, 104412 (2012).

[29] G. Chen, Dirac's "magnetic monopoles" in pyrochlore ice $U(1)$ spin liquids: Spectrum and classification, Phys. Rev. B **96**, 195127 (2017).

[30] G. Chen, "Magnetic monopole" condensation of the pyrochlore ice U(1) quantum spin liquid: Application to $Pr_2Ir_2O_7$ and $Yb_2Ti_2O_7$, Phys. Rev. B **94**, 205107 (2016).

[31] J.-J. Wen, S. M. Koohpayeh, K. A. Ross, B. A. Trump, T. M. McQueen, K. Kimura, S. Nakatsuji, Y. Qiu, D. M. Pajerowski, J. R. D. Copley, and C. L. Broholm, Disordered Route to the Coulomb Quantum Spin Liquid: Random Transverse Fields on Spin Ice in $Pr_2Zr_2O_7$, Phys. Rev. Lett. **118**, 107206 (2017).

[32] D. E. MacLaughlin, O. O. Bernal, L. Shu, J. Ishikawa, Y. Matsumoto, J.-J. Wen, M. Mourigal, C. Stock, G. Ehlers, C. L. Broholm, Yo Machida, K. Kimura, S. Nakatsuji, Y. Shimura, and T. Sakakibara, Unstable spin-ice order in the stuffed metallic pyrochlore $Pr_{2+x}Ir_{2-x}O_{7-\delta}$, Phys. Rev. B **92**, 054432 (2015).

[33] C. Liu, Y.-D. Li, and G. Chen, Selective measurements of intertwined multipolar orders: Non-Kramers doublets on a triangular lattice, Phys. Rev. B **98**, 045119 (2018).

[34] J. D. Thompson, P. A. McClarty, D. Prabhakaran, I. Cabrera, T. Guidi, and R. Coldea, Quasiparticle Breakdown and Spin Hamiltonian of the Frustrated Quantum Pyrochlore $Yb_2Ti_2O_7$ in a Magnetic Field, Phys. Rev. Lett. **119**, 057203 (2017).

[35] H. Yan, O. Benton, L. Jaubert, and N. Shannon, Theory of multiple-phase competition in pyrochlore magnets with anisotropic exchange with application to $Yb_2Ti_2O_7$, $Er_2Ti_2O_7$, and $Er_2Sn_2O_7$, Phys. Rev. B **95**, 094422 (2017).

[36] L. Savary, K. A. Ross, B. D. Gaulin, J. P. C. Ruff, and L. Balents, Order by Quantum Disorder in $Er_2Ti_2O_7$, Phys. Rev. Lett. **109**, 167201 (2012).

[37] M. E. Zhitomirsky, M. V. Gvozdikova, P. C. W. Holdsworth, and R. Moessner, Quantum Order by Disorder and Accidental Soft Mode in $Er_2Ti_2O_7$, Phys. Rev. Lett. **109**, 077204 (2012).

[38] K. A. Ross, Y. Qiu, J. R. D. Copley, H. A. Dabkowska, and B. D. Gaulin, Order by Disorder Spin Wave Gap in the XY Pyrochlore Magnet $Er_2Ti_2O_7$, Phys. Rev. Lett. **112**, 057201 (2014).

[39] J. G. Rau, S. Petit, and M. J. P. Gingras, Order by virtual crystal field fluctuations in pyrochlore XY antiferromagnets, Phys. Rev. B **93**, 184408 (2016).

[40] Y. Li, H. Liao, Z. Zhang, S. Li, F. Jin, L. Ling, L. Zhang, Y. Zou, L. Pi, Z. Yang, J. Wang, Z. Wu, and Q. Zhang, Gapless quantum spin liquid ground state in the two-dimensional spin-1/2 triangular antiferromagnet $YbMgGaO_4$, Sci. Rep. **5**, 16419 (2015).

[41] Y. Shen, Y.-D. Li, H. Wo, Y. Li, S. Shen, B. Pan, Q. Wang, H. C. Walker, P. Steffens, M. Boehm, Y. Hao, D. L. Quintero-Castro, L. W. Harriger, M. D. Frontzek, L. Hao, S. Meng, Q. Zhang, G. Chen, and J. Zhao, Evidence for a spinon fermi surface in a triangular-lattice quantum-spin-liquid candidate, Nature (London) **540**, 559 (2016).

[42] X. Zhang, F. Mahmood, M. Daum, Z. Dun, J. A. M. Paddison, N. J. Laurita, T. Hong, H. Zhou, N. P. Armitage, and M. Mourigal, Hierarchy of Exchange Interactions in the Triangular-Lattice Spin Liquid $YbMgGaO_4$, Phys. Rev. X **8**, 031001 (2018).

[43] Y.-D. Li, Y.-M. Lu, and G. Chen, Spinon Fermi surface $U(1)$ spin liquid in the spin-orbit-coupled triangular-lattice Mott insulator $YbMgGaO_4$, Phys. Rev. B **96**, 054445 (2017).

[44] Y.-D. Li, Y. Shen, Y. Li, J. Zhao, and G. Chen, Effect of spin-orbit coupling on the effective-spin correlation in $YbMgGaO_4$, Phys. Rev. B **97**, 125105 (2018).

[45] Y. Xu, J. Zhang, Y. S. Li, Y. J. Yu, X. C. Hong, Q. M. Zhang, and S. Y. Li, Absence of Magnetic Thermal Conductivity in the Quantum Spin-Liquid Candidate $YbMgGaO_4$, Phys. Rev. Lett. **117**, 267202 (2016).

[46] J. A. M. Paddison, M. Daum, Z. Dun, G. Ehlers, Y. Liu, M. B. Stone, H. Zhou, and M. Mourigal, Continuous excitations of the triangular-lattice quantum spin liquid $YbMgGaO_4$, Nat. Phys. **13**, 117 (2017).

[47] Z. Zhu, P. A. Maksimov, S. R. White, and A. L. Chernyshev, Disorder-Induced Mimicry of a Spin Liquid in $YbMgGaO_4$, Phys. Rev. Lett. **119**, 157201 (2017).

[48] Z. Zhu, P. A. Maksimov, S. R. White, and A. L. Chernyshev, Topography of Spin Liquids on a Triangular Lattice, Phys. Rev. Lett. **120**, 207203 (2018).

[49] P. A. Maksimov, Z. Zhu, S. R. White, and A. L. Chernyshev, Anisotropic-Exchange Magnets on a Triangular Lattice: Spin Waves, Accidental Degeneracies, and Dual Spin Liquids, Phys. Rev. X **9**, 021017 (2019).

[50] Y. Shen, Y.-D. Li, H. C. Walker, P. Steffens, M. Boehm, X. Zhang, S. Shen, H. Wo, G. Chen, and J. Zhao, Fractionalized excitations in the partially magnetized spin liquid candidate $YbMgGaO_4$, Nat. Commun. **9**, 4138 (2018).

[51] I. Kimchi, A. Nahum, and T. Senthil, Valence Bonds in Random Quantum Magnets: Theory And Application to $YbMgGaO_4$, Phys. Rev. X **8**, 031028 (2018).

[52] Y. Li, D. Adroja, R. I. Bewley, D. Voneshen, A. A. Tsirlin, P. Gegenwart, and Q. Zhang, Crystalline Electric-Field Randomness in the Triangular Lattice Spin-Liquid $YbMgGaO_4$, Phys. Rev. Lett. **118**, 107202 (2017).

[53] Y. Li, D. Adroja, P. K. Biswas, P. J. Baker, Q. Zhang, J. Liu, A. A. Tsirlin, P. Gegenwart, and Q. Zhang, Muon Spin Relaxation Evidence for the U(1) Quantum Spin-Liquid Ground State in the Triangular Antiferromagnet $YbMgGaO_4$, Phys. Rev. Lett. **117**, 097201 (2016).

[54] F.-Y. Li, Y.-D. Li, Y. Yu, A. Paramekanti, and G. Chen, Kitaev materials beyond iridates: Order by quantum disorder and Weyl magnons in rare-earth double perovskites, Phys. Rev. B **95**, 085132 (2017).

[55] Y. Okamoto, M. Nohara, H. Aruga-Katori, and H. Takagi, Spin-Liquid State in the $S = 1/2$ Hyperkagome Antiferromagnet $Na_4Ir_3O_8$, Phys. Rev. Lett. **99**, 137207 (2007).

[56] M. J. Lawler, H.-Y. Kee, Y. B. Kim, and A. Vishwanath, Topological Spin Liquid on the Hyperkagome Lattice Of $Na_4Ir_3O_8$, Phys. Rev. Lett. **100**, 227201 (2008).

[57] G. Chen and L. Balents, Spin-orbit effects in $Na_4Ir_3O_8$: A hyper-kagome lattice antiferromagnet, Phys. Rev. B **78**, 094403 (2008).

[58] G. Jackeli and G. Khaliullin, Mott Insulators in The Strong Spin-Orbit Coupling Limit: From Heisenberg to a Quantum Compass And Kitaev Models, Phys. Rev. Lett. **102**, 017205 (2009).

[59] J. Chaloupka, G. Jackeli, and G. Khaliullin, Kitaev-Heisenberg Model on a Honeycomb Lattice: Possible Exotic Phases in Iridium Oxides A_2IrO_3, Phys. Rev. Lett. **105**, 027204 (2010).

[60] J. Chaloupka, G. Jackeli, and G. Khaliullin, Zigzag Magnetic Order in the Iridium Oxide Na_2IrO_3, Phys. Rev. Lett. **110**, 097204 (2013).

[61] T. Takayama, A. Kato, R. Dinnebier, J. Nuss, H. Kono, L. S. I. Veiga, G. Fabbris, D. Haskel, and H. Takagi, Hyperhoneycomb Iridate β-Li_2IrO_3 as a Platform for Kitaev Magnetism, Phys. Rev. Lett. **114**, 077202 (2015).

[62] K. A. Modic, T. E. Smidt, I. Kimchi, N. P. Breznay, A. Biffin, S. Choi, R. D. Johnson, R. Coldea, P. Watkins-Curry, G. T. McCandless, J. Y. Chan, F. Gandara, Z. Islam, A. Vishwanath, A. Shekhter, R. D. McDonald, and J. G. Analytis, Realization of a three-dimensional spin anisotropic harmonic honeycomb iridate, Nat. Commun. **5**, 4203 (2014).

[63] A. Bertin, Y. Chapuis, P. D. de Réotie, and A. Yaouanc, Crystal electric field in the $R_2Ti_2O_7$ pyrochlore compounds, J. Phys.: Condens. Matter **24**, 256003 (2012).

[64] The singlet-doublet crystal-field scheme considered here is compatible with the cubic crystal-field environment. Taking the O_h crystal-field environment for example, as the O_h group is the parent group of D_{3d}, it is possible that at least the one-dimensional (A_{1g} or A_{2g}) representations and the two-dimensional (E_g) representations of the D_{3d} group still remain in the O_h cases. Indeed we find that these representations persist at least for $J = 4$ and 6 cases, which are relevant for Pr-, Tm-, or Tb-based systems.

[65] A. Joshi, M. Ma, F. Mila, D. N. Shi, and F. C. Zhang, Elementary excitations in magnetically ordered systems with orbital degeneracy, Phys. Rev. B **60**, 6584 (1999).

[66] Y. Shen, C. Liu, Y. Qin, S. Shen, Y.-D. Li, R. Bewley, A. Schneidewind, G. Chen, and J. Zhao, "Hidden order" and its quantum excitations in the triangular-lattice magnet $TmMgGaO_4$, arXiv:1810.05054.

[67] T. Giamarchi, Ch. Ruegg, and O. Tchernyshyov, Bose-Einstein condensation in magnetic insulators, Nat. Phys. **4**, 198 (2008).

[68] G. Chen, L. Balents, and A. P. Schnyder, Spin-Orbital Singlet and Quantum Critical Point on the Diamond Lattice: $FeSc_2S_4$, Phys. Rev. Lett. **102**, 096406 (2009).

[69] G. Chen, A. P. Schnyder, and L. Balents, Excitation spectrum and magnetic field effects in a quantum critical spin-orbital system: The case of $FeSc_2S_4$, Phys. Rev. B **80**, 224409 (2009).

[70] G. Khaliullin, Excitonic Magnetism in Van Vleck–Type d^4 Mott Insulators, Phys. Rev. Lett. **111**, 197201 (2013).

[71] A. Akbari and G. Khaliullin, Magnetic excitations in a spin-orbit-coupled d^4 Mott insulator on the square lattice, Phys. Rev. B **90**, 035137 (2014).

[72] J. Chaloupka and G. Khaliullin, Doping-Induced Ferromagnetism and Possible Triplet Pairing in d^4 Mott Insulators, Phys. Rev. Lett. **116**, 017203 (2016).

[73] S.-M. Souliou, J. Chaloupka, G. Khaliullin, G. Ryu, A. Jain, B. J. Kim, M. Le Tacon, and B. Keimer, Raman Scattering from Higgs Mode Oscillations in the Two-Dimensional Antiferromagnet Ca_2RuO_4, Phys. Rev. Lett. **119**, 067201 (2017).

[74] F.-Y. Li and G. Chen, Emergent quantum criticality from spin-orbital entanglement in d^8 mott insulators: The case of a diamond lattice antiferromagnet, arXiv:1808.06154.

[75] J. Zhang, K. Fritsch, Z. Hao, B. V. Bagheri, M. J. P. Gingras, G. E. Granroth, P. Jiramongkolchai, R. J. Cava, and B. D. Gaulin, Neutron spectroscopic study of crystal field excitations in $Tb_2Ti_2O_7$ and $Tb_2Sn_2O_7$, Phys. Rev. B **89**, 134410 (2014).

[76] A. J. Princep, H. C. Walker, D. T. Adroja, D. Prabhakaran, and A. T. Boothroyd, Crystal field states of Tb^{3+} in the pyrochlore spin liquid $Tb_2Ti_2O_7$ from neutron spectroscopy, Phys. Rev. B **91**, 224430 (2015).

[77] I. Mirebeau, P. Bonville, and M. Hennion, Magnetic excitations in $Tb_2Sn_2O_7$ and $Tb_2Ti_2O_7$ as measured by inelastic neutron scattering, Phys. Rev. B **76**, 184436 (2007).

[78] H. R. Molavian, M. J. P. Gingras, and B. Canals, Dynamically Induced Frustration as a Route to a Quantum Spin Ice State in $Tb_2Ti_2O_7$ Via Virtual Crystal Field Excitations and Quantum Many-Body Effects, Phys. Rev. Lett. **98**, 157204 (2007).

[79] J. S. Gardner, A. Keren, G. Ehlers, C. Stock, E. Segal, J. M. Roper, B. Fåk, M. B. Stone, P. R. Hammar, D. H. Reich *et al.*, Dynamic frustrated magnetism in $Tb_2Ti_2O_7$ at 50 mK, Phys. Rev. B **68**, 180401(R) (2003).

[80] J. S. Gardner, S. R. Dunsiger, B. D. Gaulin, M. J. P. Gingras, J. E. Greedan, R. F. Kiefl, M. D. Lumsden, W. A. MacFarlane, N. P. Raju, J. E. Sonier, I. Swainson, and Z. Tun, Cooperative Paramagnetism in the Geometrically Frustrated Pyrochlore Antiferromagnet $Tb_2Ti_2O_7$, Phys. Rev. Lett. **82**, 1012 (1999).

[81] I. Mirebeau, A. Apetrei, J. Rodríguez-Carvajal, P. Bonville, A. Forget, D. Colson, V. Glazkov, J. P. Sanchez, O. Isnard, and E. Suard, Ordered Spin Ice State and Magnetic Fluctuations in $Tb_2Sn_2O_7$, Phys. Rev. Lett. **94**, 246402 (2005).

[82] B. D. Gaulin, J. S. Gardner, P. A. McClarty, and M. J. P. Gingras, Lack of evidence for a singlet crystal-field ground state in the magnetic pyrochlore $Tb_2Ti_2O_7$, Phys. Rev. B **84**, 140402(R) (2011).

[83] S. Petit, S. Guitteny, J. Robert, P. Bonville, C. Decorse, J. Ollivier, H. Mutka, and I. Mirebeau, Spin dynamics in highly frustrated pyrochlore magnets, EPJ Web Conf. **83**, 03012 (2015).

[84] W. Witczak-Krempa, G. Chen, Y. B. Kim, and L. Balents, Correlated quantum phenomena in the strong spin-orbit regime, Annu. Rev. Condens. Matter Phys. **5**, 57 (2014).